

DOI 10.24425/ae.2022.141683

Safety assessment of electromagnetic exposure for adult and child passengers standing on the subway platform

JIN LI , MAI LU  

Key Laboratory of Opto-Electronic Technology and Intelligent Control of Ministry of Education,
Lanzhou Jiaotong University, Gansu Province, China

e-mail: mai.lu@hotmail.com

(Received: 24.02.2022, revised: 11.05.2022)

Abstract: The objective of this work is to evaluate the safety of adult and child passengers exposed to a radio frequency (RF) source, i.e., a leaky coaxial cable (LCX) on the subway platform. An adult model, a child model, and a LCX model have been numerically designed in COMSOL Multiphysics software. The distributions of the induced electric field (E -field), specific absorption rate (SAR), magnetic field (H -field) and the head temperature increase in adult and child passenger models were calculated at 900 MHz. The induced fields in the passengers were compared with that without screen doors. The results show that the E -field, SAR and H -field in the whole body of the child are 2.00×10^{-2} V/m, 1.07×10^{-7} W/kg, and 2.94×10^{-4} A/m, respectively. The E -field, SAR and H -field in the central nervous system of the child are 1.00×10^{-2} V/m, 2.44×10^{-8} W/kg, and 2.41×10^{-4} A/m, respectively. The maximum values of the E -field, SAR and H -field in the adult passenger are 1.49–2.34 times higher than those of the child. The E -field, SAR, and H -field in the passenger models without a screen door are larger than those with a screen door. The screen door has a partial shielding effect on the RF electromagnetic field. The values of the maximum temperature that increases in adult and child head tissue are 0.2114 and 0.2111°C after waiting 6 minutes exposure, respectively. All calculated results are well below the International Commission on Non-Ionizing Radiation Protection (ICNIRP) limits for general public exposure, indicating that RF electromagnetic exposure caused by the LCX on the subway platform is not a threat to passenger's health.

Key words: electromagnetic exposure, safety assessment, SAR, subway platform

1. Introduction

Subway stations are the main hubs of urban traffic. In 2021, the average daily passenger flow of 43 cities in China exceeded 64 million [1]. Over the past decade, radio frequency (RF) radiation



© 2022. The Author(s). This is an open-access article distributed under the terms of the Creative Commons Attribution-NonCommercial-NoDerivatives License (CC BY-NC-ND 4.0, <https://creativecommons.org/licenses/by-nc-nd/4.0/>), which permits use, distribution, and reproduction in any medium, provided that the Article is properly cited, the use is non-commercial, and no modifications or adaptations are made.

levels have significantly increased in our environment. Passengers expect better and faster communication services in subway stations; with these demands, the use of wireless communication is increasing tremendously. Meanwhile, the safety of the RF electromagnetic environment of the subway platform has attracted people's attention. Some citizens and governments have shown concern of the potential health effects of public RF exposures [2].

Researchers have studied the health effects and health risks of RF electromagnetic fields on the human body, especially the central nervous system. The possible biological effects of exposure to RF electromagnetic fields in the recent studies include genotoxicity, neuronal activity, and neurotransmitters; RF electromagnetic fields can induce changes in the central nervous system nerve cells, such as neuronal cell apoptosis, and changes in the function of the nerve myelin [3,4]. Studies show that RF electromagnetic fields are absorbed into the brain to such an extent that it can affect the activity of neurons [5]. The World Health Organization's International Agency for Research on Cancer (IARC) designated RF electromagnetic fields as Group 2B, i.e., possibly carcinogenic to humans [6]. Passengers standing on the subway platform are exposed to the RF electromagnetic field emitted by the subway wireless communication radiation source. It is very necessary to study the safety of electromagnetic exposure suffered by passengers.

The electromagnetic field distribution in the human tissue is usually obtained with numerical calculations because the direct measurement in the human tissue is impossible due to human ethical issues. The finite element method (FEM) is the most widely used method to compute electromagnetic fields in biological tissues [7–9]. The establishment of the human numerical model depends on the biological dielectric parameters of human tissue. The dielectric properties of human tissue are age-dependent due to the increase in the size and number of cells while the proportion of water content decreases in the development of human tissue [10–12]. Some studies on the RF energy absorption of children and adults in the electromagnetic environment have been conducted [13–16]. The absorbed energy distribution and the temperature of the child's head model exposed to the mobile phone RF electromagnetic field are studied in Reference [16], and the study shows that a significant increase is evident in the amount of absorbed energy in the brain, which is related to dielectric parameters. Subway platform passengers, especially children, are exposed to the RF electromagnetic environment, and their health risk is an important issue.

The public is usually unaware of the potential risk of exposure to electromagnetic fields, and in many cases, they cannot take precautions to avoid exposure. On this basis, the International Commission on Non-Ionizing Radiation Protection (ICNIRP) recommended more stringent exposure restrictions for the public than those of the occupationally exposed population [17]. Recently, with the evolution of telecommunications technology and the significant increase in the RF radiation level in public places, public exposure assessment is imperative [18, 19]. Some researchers measure RF exposure in public places including public transportation hubs [20, 21], such as exposure measurements at railway stations [22] and RF exposure inside the metro tube infrastructure [23]. The results of these studies showed comparatively high exposure from civil communication bands and the major source of exposure in the subway was GSM900. Most previous studies focused on the coverage of the wireless system in subways or a high-speed railway environment [24], and little information has been published on electromagnetic exposure safety in the rail transit system, except for recent studies [8, 25, 26]. The research on the general public electromagnetic exposure of subway passengers, especially children, is limited.

In this work, we use COMSOL Multiphysics software to model and solve the FEM models. First, we calculated the distributions of the E -field, SAR, H -field, and the head temperature increase in adult and child passenger models exposed to the RF electromagnetic field emitted from a leaky coaxial cable (LCX) on the subway platform at 900 MHz. We particularly focus on the induced fields in the central nervous system. Then, the effect of subway platform screen doors on RF electromagnetic exposure is analyzed, and the effectiveness of the simulation is verified by measurement. Finally, the calculation results are compared with the ICNIRP limits for general public exposure to access the safety of the RF electromagnetic environment on the subway platform for adult and child passengers.

2. Theory and models

2.1. Exposure source

The LCX with vertical periodic slots was designed for subway wireless communication with a frequency band of 800–2400 MHz. The LCX has a characteristic impedance of $50 \pm 2 \Omega$, and the voltage standing wave ratio (VSWR) ≤ 1.3 . The inner conductor is a copper tube, the outer conductor is a corrugated copper tube, and the insulation material is fire-proof physical foamed polyethylene with a permittivity of 1.26. The structure of the LCX is shown in Figs. 1(a)–1(c). The radius of the inner conductor and outer conductor is a and b , respectively.

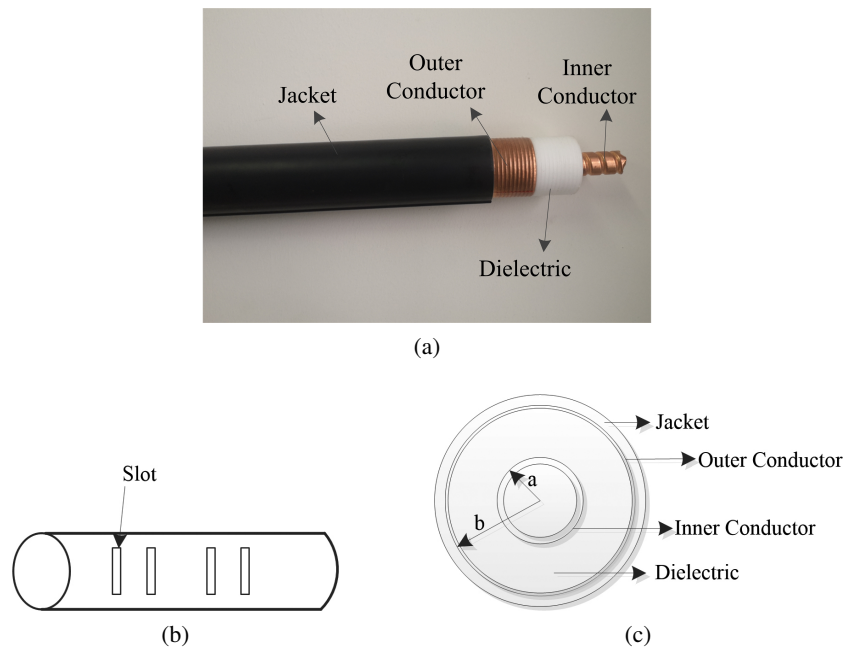


Fig. 1. Structure of the LCX: image of the LCX (a); slots on the outer conductor (b); cross section of the LCX (c)

We calculated the same LCX as Reference [27] in COMSOL to verify the effectiveness of COMSOL software in cable simulation; it has four slots in each period, and the slot period is 360 mm. The cable's parameters are $a = 8$ mm, and $b = 22.65$ mm, with a characteristic impedance of 50Ω . The slot length and width are 24.3 mm and 2.53 mm, respectively. The results are shown in Table 1 which clearly shows that the error is 3%. These results are in good agreement, thereby indicating that the reliability of the LCX modeling and calculation in this work has been proven.

Table 1. Comparison of simulation values between this paper and Reference [27]

	Coupling loss
Reference [27]	69 dB
This paper	67 dB

The model of the LCX on the subway platform was established as shown in Fig. 2. Each period has seven vertical slots. Each vertical slot has a size of $19.5 \text{ mm} \times 3 \text{ mm}$. The slot period length is 246 mm, and the LCX is 2 706 mm long with 11 slot periods. As shown in Table 2, the simulation results of the LCX indicate that the LCX model is a suitable design requirement.

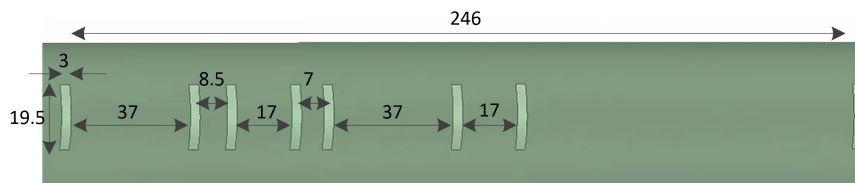


Fig. 2. Structural dimension of LCX (unit: mm)

Table 2. Simulation results of the LCX

Frequency(MHz)	Transmission loss (dB/100m)		Coupling loss (dB)		VSWR
	Standard value	Simulation value	Standard value	Simulation value	
900	2.6	2.30	74	72.85	1.0072
1 800	4.3	4.10	72	72.20	1.0246
2 400	6.3	5.51	70	68.94	1.0110

2.2. Theory

The LCX distributes radio waves to the subway platform. The propagation of electromagnetic waves of the LCX follows Maxwell's equations. Hence, the electric field strength and magnetic

field strength are calculated according to Maxwell's equations. Differential forms of Maxwell's equations are (1)–(4), as follows:

$$\nabla \times H = J + \frac{\partial D}{\partial t}, \quad (1)$$

$$\nabla \times E = -\frac{\partial B}{\partial t}, \quad (2)$$

$$\nabla \cdot D = \rho, \quad (3)$$

$$\nabla \cdot B = 0, \quad (4)$$

where: H is the magnetic field strength (A/m), E is the electric field strength (V/m), J is the current density (A/m²), B is the magnetic induction strength (T), D is the electric flux density (C/m²), and ρ is the volume density of charge (C/m³).

Constitutive relations of Maxwell's equations are as follows:

$$B = \mu H, \quad (5)$$

$$D = \varepsilon E, \quad (6)$$

$$J = \sigma E, \quad (7)$$

where μ is the magnetic permeability (H/m), ε is the permittivity (F/m), and σ is the conductivity (S/m).

SAR distributions within the human tissue are usually determined through numerical calculation. The SAR is calculated as follows:

$$\text{SAR} = \frac{\sigma E^2}{2\rho} \quad (\text{W/kg}), \quad (8)$$

where σ is the conductivity (S/m), E is the induced electric field (V/m) within the human body, and ρ is the mass density (kg/m³) of the human tissue.

2.3. Adult and child passenger models

Figure 3 shows the passengers standing on the subway platform exposed to the LCX. The adult model's standing height is 1.74 m, and the child (seven years old) model's standing height is 1.278 m [28]. Each human model has a three-layer head model. The radii of scalp tissue, skull tissue, and brain tissue of the adult model are 92, 85, and 80 mm, respectively, in accordance with international standards [29]. The radii of scalp tissue, skull tissue and brain tissue of the reduced scale child model are 67, 62, and 58 mm, respectively, and are scaled down [30].

The dielectric properties of adult body tissues are obtained by a 4-Cole-Cole extrapolation [31]. The suitability of the empirical formula for children's dielectric parameters in Reference [32] has been demonstrated. The dielectric parameters of child body tissues are derived from Reference [32]. Table 3 shows the dielectric properties for the adult and child (seven years old) at 900 MHz and mass densities for human tissue. In Table 3, the dielectric properties of the brain are the average values of white matter and gray matter, and the dielectric properties of the trunk are the average values of skin, blood, muscle, and bone. Mass densities for human tissues are from Reference [33]. Figure 4 shows the adult and child models, and Fig. 5 shows the finite element mesh of adult and child models.



Fig. 3. Passengers standing on the subway platform

Table 3. Dielectric properties for adult and child at 900 MHz and mass densities for human tissues

Human tissue	Adult		Child (seven years old)		Mass density (kg/m ³)
	Conductivity (S/m)	Permittivity	Conductivity (S/m)	Permittivity	
Scalp	0.845	46.08	0.89	42.47	1125
Skull	0.143	12.454	0.36	21.97	1990
Brain	0.767	45.806	0.78	46.75	1038
Trunk	0.867	43.732	0.945	45.74	1305

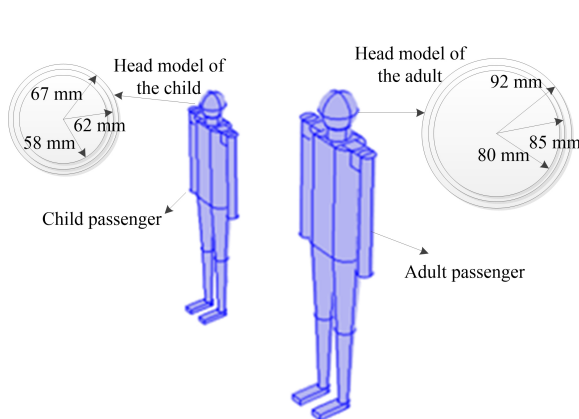


Fig. 4. Numerical models (unit: mm)

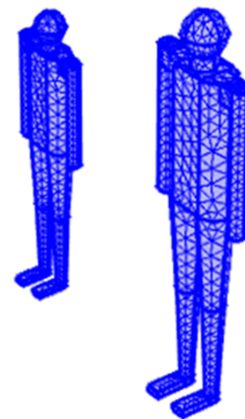


Fig. 5. Finite element mesh of numerical models

2.4. Numerical models

The numerical models with adult and child passengers, the LCX, the screen door, and air box are shown in Fig. 6. The LCX is located above the platform tunnel wall, which is 2.2 m away from the subway platform ground and 4.2 m horizontally away from the platform screen door. The adult and child passengers are standing 0.5 m away from the platform screen door. The screen door consists of a glass door with dimensions of 50 mm × 1 900 mm × 500 mm and an aluminum alloy plate above with dimensions of 50 mm × 1 900 mm × 2 000 mm. In the RF module of COMSOL software, the numerical models with an air domain were established. Then, the FEM mesh models were built with a 4 425 216 elements. The mesh models are shown in Fig. 7. The exciting power in the LCX is 22 dBm, and the operating frequency is 900 MHz.

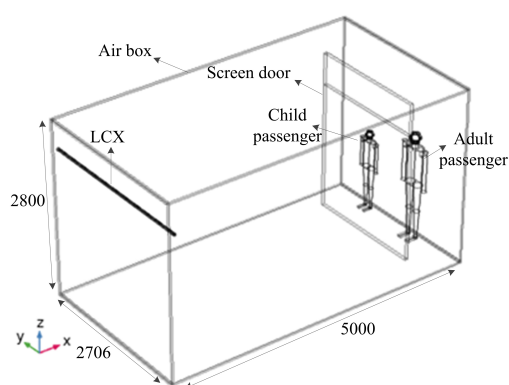


Fig. 6. Numerical models (unit: mm)

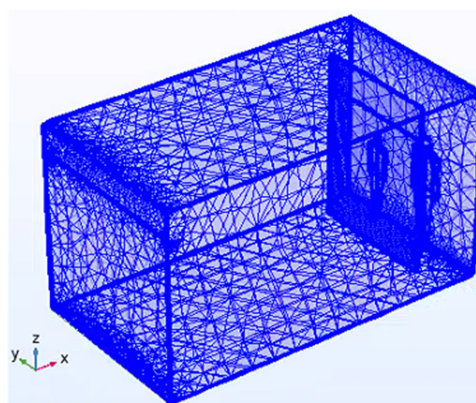


Fig. 7. Finite element mesh of numerical models

3. Simulation results and discussions

This work analyzes electromagnetic distributions in the whole body of adult passengers, and in the central nervous system. Then, energy absorptions of passenger models were compared in the following cases: with a screen door and without a screen door.

3.1. Analysis of an adult passenger

When an adult passenger stands on the subway platform, the E -field distribution, SAR distribution, and H -field distribution are as shown in Figs. 8–10. As shown in Figs. 8–10, the maximum values of the E -field, SAR, and H -field in the adult passenger are 0.04×10^{-3} V/m, 2.5×10^{-7} W/kg, and 4.38×10^{-4} A/m, respectively. The E -field, SAR, and H -field are mainly distributed in the head of the adult passenger.

We focus on the brain, i.e., the central nervous system, of the adult passenger. Figs. 11–13 show the distribution of the E -field, SAR, and H -field in the brain of the adult passenger. The maximum values of the E -field, SAR, and H -field in the brain of the adult passenger are 0.02×10^{-3} V/m, 7.19×10^{-8} W/kg, and 4.06×10^{-4} A/m, respectively. The E -field, SAR, and H -field are mainly distributed in the brain near the side of the LCX and decay rapidly in the brain.

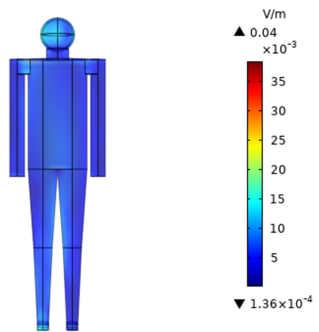


Fig. 8. *E*-field distribution in the adult body

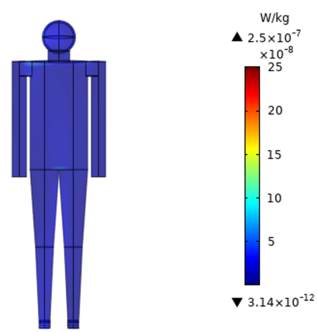


Fig. 9. SAR distribution in the adult body

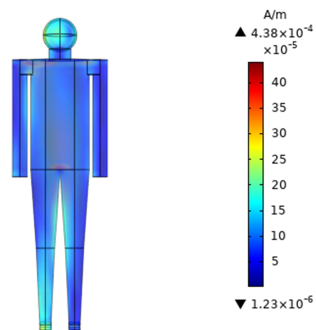


Fig. 10. *H*-field distribution in the adult body

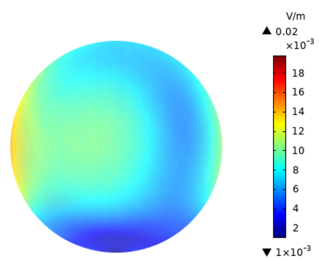


Fig. 11. *E*-field distribution in the adult brain

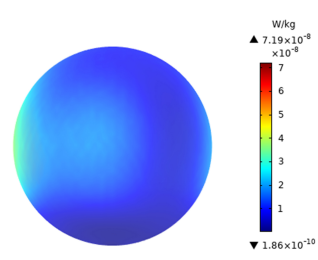


Fig. 12. SAR distribution in the adult brain

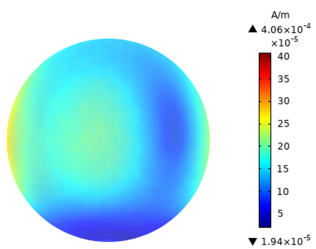


Fig. 13. *H*-field distribution in the adult brain

3.2. Analysis of a child passenger

A child passenger stands 1 m away from the adult passenger, as shown in Fig. 16. The E -field distribution, SAR distribution, and H -field distribution in the body of the child passenger are shown in Figs. 14–16, respectively. As shown in Figs. 14–16, the maximum values of the E -field, SAR and H -field in the child passenger are 2.00×10^{-2} V/m, 1.07×10^{-7} W/kg, 2.94×10^{-4} A/m, respectively. The calculation results in the body of the child passenger are less than the corresponding values in the adult passenger. The observed differences can be explained by the different dielectric parameters and the height of models of child and adult passengers.

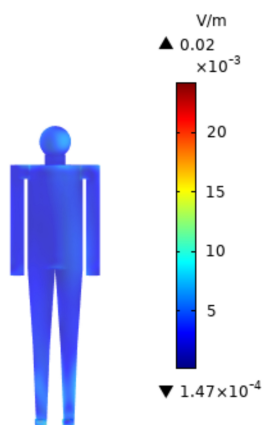
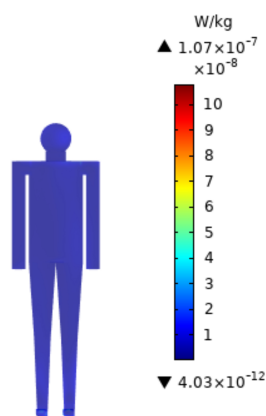
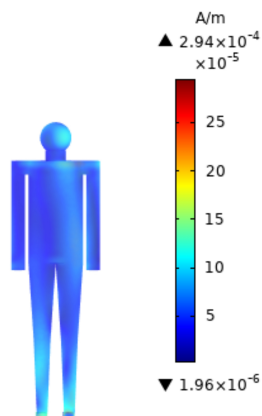
Fig. 14. E -field distribution in the child body

Fig. 15. SAR distribution in the child body

Fig. 16. H -field distribution in the child body

To further analyze the electromagnetic energy distribution in the brain of the child passenger, Figs. 17–19 show the distribution of the E -field, SAR, and H -field in the brain of the child passenger. The maximum values of the E -field, SAR, and H -field in the brain of the child passenger are 1.00×10^{-2} V/m, 2.44×10^{-8} W/kg, and 2.41×10^{-4} A/m, respectively, which are

lower than those of the adult passenger. This finding is mainly because the brain of the child is far away from the radiation source than that of the adult.

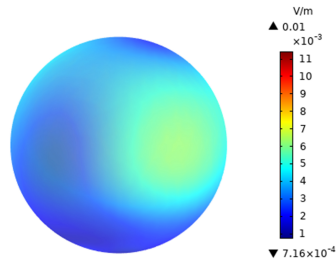


Fig. 17. *E*-field distribution in the child brain

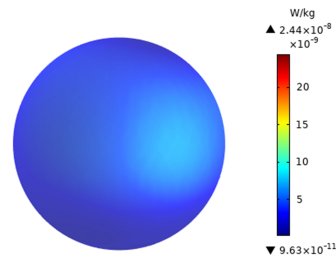


Fig. 18. SAR distribution in the child brain

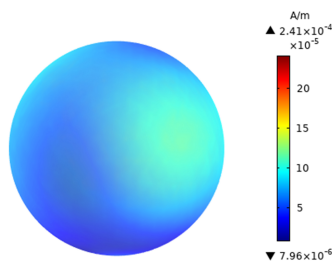


Fig. 19. *H*-field distribution in the child brain

Table 4 shows that the maximum values of the SAR, *E*-field, and *H*-field in the whole body of the adult passenger are 1.49–2.34 times higher than those of the child. Table 4 shows that the adult passenger has higher induced fields. The explanation for this observations is that although the child and adult passengers have different dielectric parameters, the adult is taller than the child and closer to the radiation source, which is hanged on the top of the wall. Results show that the child passenger does not suffer greater electromagnetic exposure risk than the adult passenger on the subway platform.

Table 4. Comparison of induced fields in the whole body of adult and child passengers

Induced fields	Adult	Child	Ratio (adult/child)
SAR (W/kg)	2.50×10^{-7}	1.07×10^{-7}	2.34
<i>E</i> -field (V/m)	4.00×10^{-2}	2.00×10^{-2}	2
<i>H</i> -field (A/m)	4.38×10^{-4}	2.94×10^{-4}	1.49

3.3. Analysis on passengers when no screen door exists

To analyze the effect of a subway platform screen door on electromagnetic exposure, the screen door is deleted from the model in Fig. 6, and electromagnetic distributions in adult and child passengers are calculated.

Table 5 shows the comparison of calculation results with and without a screen door. The screen door includes a glass door (the permittivity is 5.5, and the conductivity is 1 S/m), and aluminum alloy plate (the permittivity is 1, and the conductivity is 3.3×10^7 S/m). The distributions of the SAR, E -field, and H -field in the passenger models without the screen door are larger than those with the screen door. For the adult passenger, the ratios of induced fields with and without the screen door are 0.12–0.40. For the child passenger, the ratios of induced fields with and without the screen door are 0.19–0.44. The findings show that the screen door has partial shielding effect on the electromagnetic exposure of passengers.

Table 5. Comparison of calculation results of induced fields in passengers with and without screen door

Induced fields	Adult			Child		
	With screen door	Without screen door	Ratio (with screen door/without screen door)	With screen door	Without screen door	Ratio (with screen door/without screen door)
SAR (W/kg)	4.78×10^{-8}	4.07×10^{-7}	0.12	3.90×10^{-8}	2.09×10^{-7}	0.19
E -field (V/m)	2.00×10^{-2}	5.00×10^{-2}	0.40	1.00×10^{-2}	3.00×10^{-2}	0.33
H -field (A/m)	2.08×10^{-4}	5.70×10^{-4}	0.36	1.92×10^{-4}	4.36×10^{-4}	0.44

3.4. Comparison of calculation results with ICNIRP public exposure limits

The calculation results with a subway platform screen door are compared with ICNIRP public exposure limits in Table 6. Calculation results of adult and child passengers are well below the ICNIRP limits for public exposure.

Table 6. Comparison of calculation results with ICNIRP public exposure limits

Body tissues	E -field (V/m)	Ration (%)	SAR (W/kg)	Ration (%)	H -field (A/m)	Ration (%)
Brain of the child	1.00×10^{-2}	0.02%	2.44×10^{-8}	0.000001%	2.41×10^{-4}	0.22%
Whole body of the child	2.00×10^{-2}	0.05%	1.07×10^{-7}	0.0001%	2.94×10^{-4}	0.26%
Brain of the adult	2.00×10^{-2}	0.05%	7.19×10^{-8}	0.000004%	4.06×10^{-4}	0.37%
Whole body of the adult	4.00×10^{-2}	0.10%	2.50×10^{-7}	0.0003%	4.38×10^{-4}	0.39%
ICNIRP public exposure limits	41.25		0.08 (whole body), 2 (head)		0.111	

4. Verification of measurement and simulation

4.1. Measuring equipment and methods

A subway platform in operation in China is selected as the measurement location, and the measurement frequency band of the subway wireless communication system is 806–960 MHz. According to the electromagnetic field intensity measurement principle of the subway electromagnetic environment, the measurement equipment adopts a spectrum analyzer, electromagnetic field intensity analyzer, and antenna with an optional frequency band [34]. The measuring equipment are shown in Fig. 20. The subway platform for measurement is shown in Fig. 21. Table 7 shows the performance parameters of the measuring equipment. The passenger waiting area is

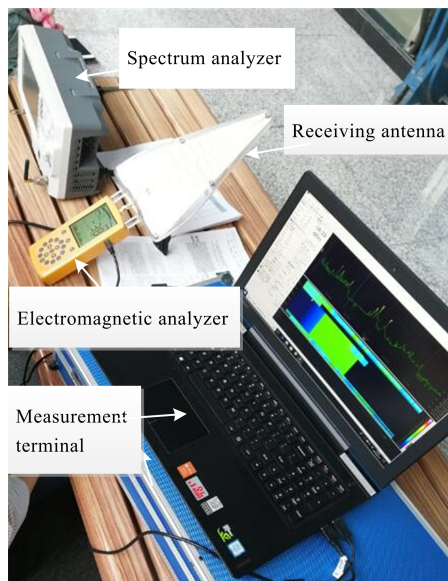


Fig. 20. Measuring equipment



Fig. 21. Subway platform for measurement

measured, and the electric field intensity of the subway platform is analyzed. The measurement position on the subway platform is shown in Fig. 22.

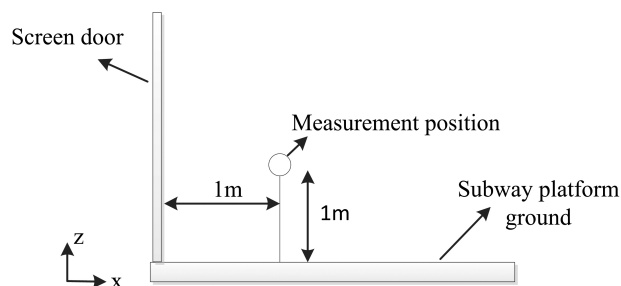


Fig. 22. Measurement position on the subway platform

Table 7. Performance parameters of measuring equipments

Equipment name	Frequency range	Measurement error	Input mode
Electromagnetic analyzer	1 MHz–9 GHz	±3 dB	Log periodic antenna
Spectrum analyzer	9 kHz–3.2 GHz	±0.8 dB	Dipole antenna

The input impedance of the measurement system is 50Ω , ignoring the cable loss between the receiving antenna and the analyzer, and the calculation formula of the electric field strength is expressed as follows [35]:

$$E = K + A + 107 + L, \quad (9)$$

where K is the antenna coefficient (dB), which is the ratio of electric field intensity to receiver port voltage, and A is the signal strength of the spectrum analyzer or electromagnetic analyzer (dBm). The difference between the measured voltage of 50Ω measuring equipment and the digital amplitude reading is 107. If there is a cable connection between the receiving antenna and electromagnetic analyzer, L is the loss value of the connecting cable (dB). The antenna gain G is usually used to calculate the antenna coefficient K , as shown in Eq. (10).

$$K = 20 \lg \left(\frac{9.76}{\lambda \sqrt{G}} \right), \quad (10)$$

where λ is the wavelength (m). The equipment is calibrated before measuring.

4.2. Measurement result

The screenshot of the measurement results of the spectrum analyzer is shown in Fig. 23. The measurement result is -36.45 dBm at 949 MHz. According to the above equations, (9) and (10), the corresponding E -field is 0.047 V/m at 949 MHz.

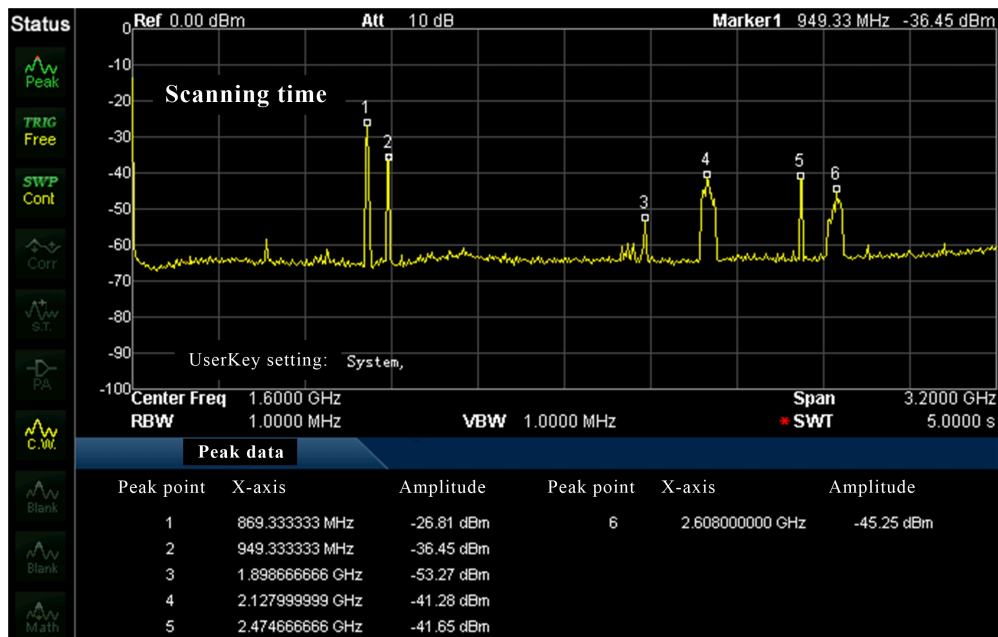


Fig. 23. Measurement results of the spectrum analyzer

4.3. Comparison of measurement and simulation results

We calculated the E -field distribution on the subway platform 1 m away from the screen door at a frequency of 949 MHz. The simulation result of the E -field distribution on the subway platform is shown in Fig. 24. The bottom of the screen door is the coordinate origin, and the simulation value of the E -field at the point (1 000 mm, 432 mm, 1 000 mm) is 0.045 V/m, which is in good agreement with the measured value.

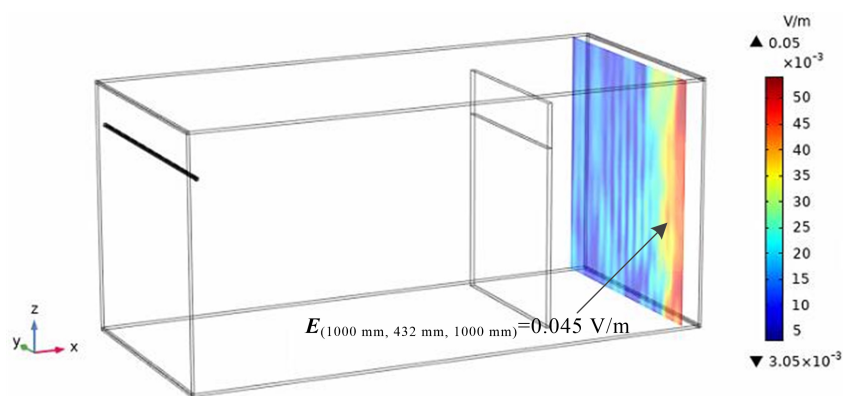


Fig. 24. Simulation results of electric field intensity on the subway platform

5. Simulation of temperature in human tissues

Human tissue exposed to the RF electromagnetic field absorbs electromagnetic radiation and may cause the temperature of human tissue to rise. This paper further studies the temperature distribution of adult brain tissue under the far-field exposure of a leaky coaxial cable. COMSOL software supports the numerical calculation of multi physical field coupling. The coupling of the RF module and biological heat transfer module is used to calculate the temperature distribution of the head tissues in adult and child passengers. The Pennes transient biothermal equation is used to calculate the temperature distribution of human tissue [36–38]. The heat transfer formula is expressed as follows [33]:

$$\rho C \frac{\partial T}{\partial t} = \nabla \times (k \nabla T) + \rho_b C_b \omega_b (T_b - T) + Q_{\text{met}} + \rho \times \text{SAR}, \quad (11)$$

where: ρ is the mass density (kg/m^3) of the human tissue, C is the specific heat capacity of tissue ($\text{J}/(\text{kg} \cdot ^\circ\text{C})$), k is thermal conductivity of tissue ($\text{W}/(\text{m} \cdot ^\circ\text{C})$), T is the temperature of the body tissue ($^\circ\text{C}$), T_b is the temperature of blood ($^\circ\text{C}$), ρ_b is the density of blood (kg/m^3), C_b is the specific heat capacity of blood ($\text{J}/(\text{kg} \cdot ^\circ\text{C})$), ω_b is the blood perfusion rate (s^{-1}), and Q_{met} is the heat source (W/m^3). Table 8 shows thermal parameters of human tissue [33]. The ambient temperature of the subway platform is set to 20°C , and the initial temperature of human tissue and blood is set to 37°C .

Table 8. Thermal parameters of human tissue

Human tissue	Thermal conductivity ($\text{W} \cdot (\text{m} \cdot ^\circ\text{C})^{-1}$)	Specific heat capacity ($\text{J} \cdot (\text{kg} \cdot ^\circ\text{C})^{-1}$)	Heat source ($\text{W} \cdot \text{m}^{-3}$)	Blood perfusion rate (s^{-1})
Skin	0.42	3600	1620	0.02
Bone	0.37	3100	610	0.000463
Brain	0.53	3650	7100	0.00883

To compare with the ICNIRP guideline limits, the electromagnetic exposure time is defined as 6 minutes [17]. The temperature distribution of xy axis sections of the adult head model after waiting for 6 minutes is shown in Fig. 25. It is found that the maximum temperature of the adult head sections is 37.2114°C , which is 0.2114°C higher than the initial temperature. As shown in Fig. 25, the brain tissue is sensitive to temperature changes, and the temperature in brain tissue increases significantly. The temperature distribution of xy axis sections of the child head model after waiting for 6 minutes is shown in Fig. 26. The maximum temperature of the child head sections is 37.2111°C , which is 0.0003°C smaller than the adult. Both temperature increases are below the thermal damage limit established by the ICNIRP guideline, that is, 1°C .

The points where the brain surface intersects with the y -axis are taken in the adult and child head models, respectively. We studied the temperature changes at these two points from 0 to 6 minutes. Temperature changes over time at two points in adult and child brain tissue are shown in Fig. 27. In 1 to 3 minutes, the temperature of the point in child brain tissue increases faster than that of the adult. In 4 to 6 minutes, the temperature of the two curves is almost the same. This shows that the temperature changes of the adult and child head tissue are almost the same.

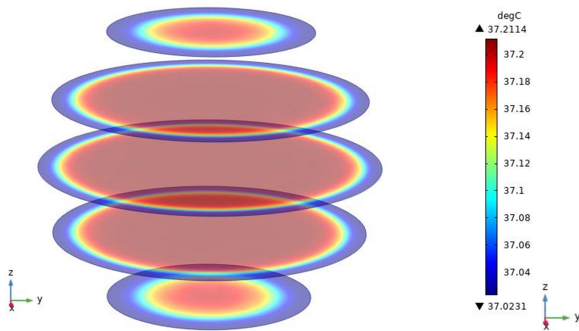


Fig. 25. Temperature distribution of xy axis sections of adult head model after waiting for 6 minutes

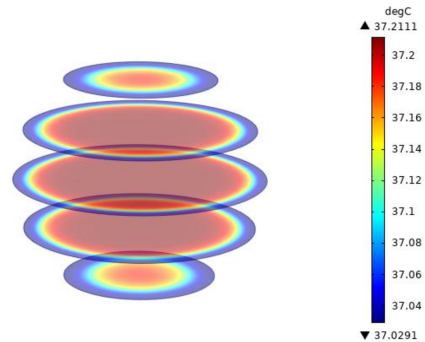


Fig. 26. Temperature distribution of xy axis sections of child head model after waiting for 6 minutes

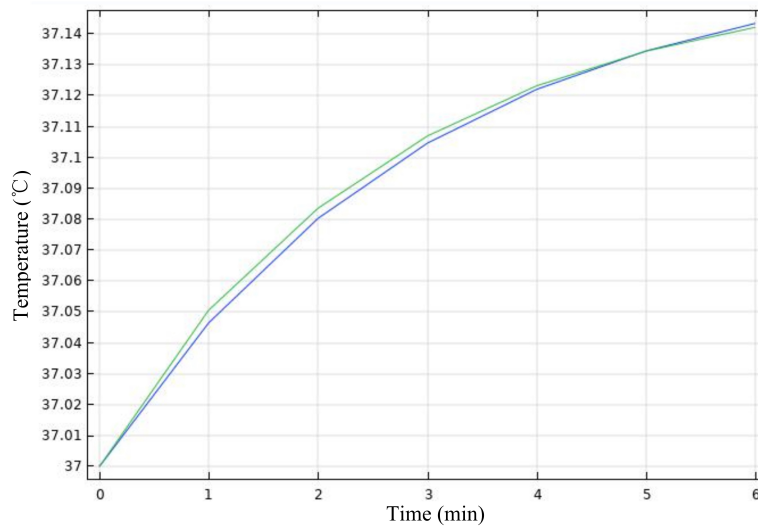


Fig. 27. Temperature changes from 0 to 6 minutes

6. Conclusions

In this work, the distributions of the induced E -field, SAR, induced H -field, and the head temperature increase in adult and child passengers were analyzed to evaluate the safety of RF electromagnetic exposure generated by the LCX on the subway platform. The conclusions are as follows:

- The calculated results of the E -field, SAR, and H -field in the adult passenger and the child passenger were analyzed. The E -field, SAR and H -field in the child body are 2.00×10^{-2} V/m, 1.07×10^{-7} W/kg, and 2.94×10^{-4} A/m, respectively, which are smaller than those of the adult body. The maximum values of electromagnetic distributions in the adult passenger are 1.49–2.34 times higher than those of the child.

- The effect of a subway platform screen door on passengers' electromagnetic exposure was analyzed. The E -field, SAR and H -field in passengers with a screen door are 0.12–0.44 times those without a screen door. Therefore, the screen door has partial shielding effect on the RF electromagnetic field. Moreover, the E -field distribution was measured on the subway platform. The simulation result is in good agreement with the measurement result.
- The temperature distribution of the adult and child passenger's head tissue was simulated. The maximum increases in the adult and child head tissue are 0.2114 and 0.2111°C after waiting 6 minutes, respectively. The temperature increases are below the thermal damage limit, that is, 1°C, established by ICNIRP guidelines.
- All calculated results were compared with ICNIRP public exposure limits. The maximum values of the E -field, SAR and H -field in passenger models are well below the ICNIRP limits for general public exposure. The results indicate that the health of passengers on subway platforms is not threatened by RF radiation from the LCX at 900 MHz.

Acknowledgements

This work is supported in part by the National Natural Science Foundation of China under Grant 51867014, in part by the Natural Science Foundation of Gansu Province, China under Grant 20JR10RA217, and in part by the Opening Foundation of Key Laboratory of Opto-Electronic Technology and Intelligent Control (Lanzhou Jiaotong University), Ministry of Education, China under Grant KFKT2020-14.

References

- [1] <https://www.163.com/dy/article/H08UC3PI0514810F.html>, accessed February 2022.
- [2] Verbeek J., Oftedal G., Feychting M., Rongen E., *Prioritizing health outcomes when assessing the effects of exposure to radiofrequency electromagnetic fields: A survey among experts*, Environment International, vol. 146, no. 1, pp. 1–6 (2020), DOI: [10.1016/j.envint.2020.106300](https://doi.org/10.1016/j.envint.2020.106300).
- [3] Ju H.K., Lee J.K., Kim H.G., *Possible Effects of Radiofrequency Electromagnetic Field Exposure on Central Nerve System*, Biomolecules and Therapeutics, vol. 27, no. 3, pp. 265–275 (2019), DOI: [10.4062/biomolther.2018.152](https://doi.org/10.4062/biomolther.2018.152).
- [4] Jiang D.P., Li J.H., Zhang J., *Long-term electromagnetic pulse exposure induces Abeta deposition and cognitive dysfunction through oxidative stress and overexpression of APP and BACE1*, Brain Research, vol. 1642, no. 1, pp. 10–19 (2016), DOI: [10.1016/j.brainres.2016.02.053](https://doi.org/10.1016/j.brainres.2016.02.053).
- [5] Hinrikus H., Bachmann M., Lass J., *Understanding physical mechanism of low-level microwave radiation effect*, International Journal of Radiation Biology, vol. 94, no. 10, pp. 877–882 (2018), DOI: [10.1080/09553002.2018.1478158](https://doi.org/10.1080/09553002.2018.1478158).
- [6] Baan R., Grosse Y., Lauby-Secretan B., El Ghissassi F., *Carcinogenicity of radiofrequency electromagnetic fields*, Lancet Oncology, vol. 12, no. 7, pp. 624–626 (2011), DOI: [10.1016/S1470-2045\(11\)70147-4](https://doi.org/10.1016/S1470-2045(11)70147-4).
- [7] Qi X.Z., Lu M., *Study on the distribution of SAR and temperature in human brain during radio-frequency cosmetic treatment*, Archives of Electrical Engineering, vol. 70, no. 1, pp. 115–127 (2021), DOI: [10.24425/ae.2021.136056](https://doi.org/10.24425/ae.2021.136056).
- [8] Tian R., Lu M., *Safety assessment of electromagnetic exposure in high-speed train carriage with full passengers*, Annals of Work Exposures and Health, vol. 64, no. 8, pp. 838–851 (2020), DOI: [10.1093/annweh/wxaa048](https://doi.org/10.1093/annweh/wxaa048).

- [9] Gas P., Wyszowska J., *Influence of multi-tine electrode configuration in realistic hepatic RF ablative heating*, Archives of Electrical Engineering, vol. 68, no. 3, pp. 521–533 (2019), DOI: [10.24425/ae.2019.129339](https://doi.org/10.24425/ae.2019.129339).
- [10] Stankovi V., Jovanovi D., Krsti D., *Temperature distribution and Specific Absorption Rate inside a child's head*, International Journal of Heat and Mass Transfer, vol. 104, no. 1, pp. 559–565 (2017), DOI: [10.1016/j.ijheatmasstransfer.2016.08.094](https://doi.org/10.1016/j.ijheatmasstransfer.2016.08.094).
- [11] Peyman A., Rezazadeh A.A., Gabriel C., *Changes in the dielectric properties of rat tissue as a function of age at microwave frequencies*, Physics in Medicine and Biology, vol. 46, no. 12, pp. 1617–1629 (2001), DOI: [10.1088/0031-9155/55/15/N02](https://doi.org/10.1088/0031-9155/55/15/N02).
- [12] Peyman A., Gabriel C., Grant E.H., *Variation of the dielectric properties of tissues with age: the effect on the values of SAR in children when exposed to walkie-talkie devices*, Physics in Medicine and Biology, vol. 54, no. 1, pp. 227–241 (2009), DOI: [10.1088/0031-9155/54/2/004](https://doi.org/10.1088/0031-9155/54/2/004).
- [13] Foster K.R., Chou C.K., *Are Children More Exposed to Radio Frequency Energy from Mobile Phones Than Adults?*, IEEE Access, vol. 2014, no. 2, pp. 1497–1509 (2014), DOI: [10.1109/ACCESS.2014.2380355](https://doi.org/10.1109/ACCESS.2014.2380355).
- [14] Gandhi O.P., *Yes the children are more exposed to radiofrequency energy from mobile telephones than adults*, IEEE Access, vol. 2015, no. 3, pp. 985–988 (2015), DOI: [10.1109/ACCESS.2015.2438782](https://doi.org/10.1109/ACCESS.2015.2438782).
- [15] Morris R.D., Morgan L.L., Davis D., *Children Absorb Higher Doses of Radio Frequency Electromagnetic Radiation from Mobile Phones Than Adults*, IEEE Access, vol. 2015, no. 3, pp. 2379–2387 (2015), DOI: [10.1109/ACCESS.2015.2478701](https://doi.org/10.1109/ACCESS.2015.2478701).
- [16] Stankovi V., Jovanovi D., Krsti D., Markovi V., Cvetkovi N., *Temperature distribution and specific absorption rate inside a child's head*, International Journal of Heat and Mass Transfer, vol. 104, no. 1, pp. 559–565 (2017), DOI: [10.1016/j.ijheatmasstransfer.2016.08.094](https://doi.org/10.1016/j.ijheatmasstransfer.2016.08.094).
- [17] ICNIRP, *Guidelines for Limiting Exposure to Electromagnetic Fields (100 kHz to 300 GHz)*, Health Physics, vol. 118, no. 5, pp. 483–524 (2020), DOI: [10.1097/HP.0000000000001210](https://doi.org/10.1097/HP.0000000000001210).
- [18] Hardell L., *World Health Organization, radiofrequency radiation and health - a hard nut to crack (Review)*, International Journal of Oncology, vol. 51, no. 2, pp. 405–413 (2017), DOI: [10.3892/ijo.2017.4046](https://doi.org/10.3892/ijo.2017.4046).
- [19] Tsa B., Db B., Arm B., *Biological effects of non-ionizing electromagnetic fields: Two sides of a coin*, Progress in Biophysics and Molecular Biology, vol. 141, no. 1, pp. 25–36 (2019), DOI: [10.1016/j.pbiomolbio.2018.07.009](https://doi.org/10.1016/j.pbiomolbio.2018.07.009).
- [20] Ayugi G., Kisolo A., Ireeta T.W., *Temporal variation of radiofrequency electromagnetic field exposure from mobile phone base stations in sensitive environments*, IOSR Journal of Applied Physics, vol. 9, no. 5, pp. 9–15 (2020), DOI: [10.9790/4861-0905010915](https://doi.org/10.9790/4861-0905010915).
- [21] Carlberg M., Hedendahl L., Koppel T., *High ambient radiofrequency radiation in Stockholm city, Sweden*, Oncology letters, vol. 17, no. 2, pp. 1777–1783 (2018), DOI: [10.3892/ol.2018.9789](https://doi.org/10.3892/ol.2018.9789).
- [22] Hardell L., Koppel T., Carlberg M., *Radiofrequency radiation at Stockholm Central Railway Station in Sweden and some medical aspects on public exposure to RF fields*, International Journal of Oncology, vol. 49, no. 2, pp. 1315–1324 (2016), DOI: [10.3892/ijo.2016.3657](https://doi.org/10.3892/ijo.2016.3657).
- [23] Gryz K., Karpowicz J., *Radiofrequency electromagnetic radiation exposure inside the metro tube infrastructure in Warszawa*, Electromagnetic Biology and Medicine, vol. 34, no. 3, pp. 265–273 (2015), DOI: [10.3109/15368378.2015.1076447](https://doi.org/10.3109/15368378.2015.1076447).
- [24] Zhang B., Zhong Z., He R., *Multi-User channels with large-scale antenna arrays in a subway environment: characterization and modeling*, IEEE Access, vol. 5, no. 1, pp. 23613–23625 (2017), DOI: [10.1109/ACCESS.2017.2764621](https://doi.org/10.1109/ACCESS.2017.2764621).

- [25] Yang C.Q., Lu M., *Safety evaluation for a high signal operator with electric field exposure induced by contact wires*, Archives of Electrical Engineering, vol. 70, no. 2, pp. 431–444 (2021), DOI: [10.24425/aec.2021.136994](https://doi.org/10.24425/aec.2021.136994).
- [26] Jalilian H., Najafi K., Monazzam M.R., *Occupational Exposure of Train Drivers to Static and Extremely Low Frequency Magnetic Fields in Tehran Subway*, Jundishapur Journal of Health Sciences, vol. 9, no. 4, pp. 1–8 (2017), DOI: [10.5812/jjhs.14329](https://doi.org/10.5812/jjhs.14329).
- [27] Wang J.H., Mei K.K., *Design of leaky coaxial cables with periodic slots*, Radio Science, vol. 37, no. 5, pp. 1–10 (2002), DOI: [10.1029/2000RS002534](https://doi.org/10.1029/2000RS002534).
- [28] Standardization Administration of China, *Human dimensions of Chinese minors*, GB/T 26158-2010 (2011).
- [29] Rush S., *Current distribution in the brain from surface electrodes*, Anesthesia & Analgesia, vol. 47, no. 6, pp. 717–723 (1968).
- [30] Gandhi O.P., Lazzi G., Furse C.M., *Electromagnetic absorption in the human head and neck for mobile telephones at 835 and 1900 MHz*, IEEE Transactions on Microwave Theory and Techniques, vol. 44, no. 10, pp. 1884–1897 (1996), DOI: [10.1109/22.539947](https://doi.org/10.1109/22.539947).
- [31] Gabriel C., Gabriel S., Corthout E., *The dielectric properties of biological tissues: I. Literature survey*, Phys. Med. Biol., vol. 41, no. 11, pp. 2231–49 (1996).
- [32] Wang J., Fujiwara O., Watanabe S., *Approximation of aging effect on dielectric tissue properties for SAR assessment of mobile telephones*, IEEE Transactions on Electromagnetic Compatibility, vol. 48, no. 2, pp. 408–413 (2006), DOI: [10.1109/TEMC.2006.874085](https://doi.org/10.1109/TEMC.2006.874085).
- [33] Bhargava D., Leeprechanon N., Rattanadecho P., *Specific absorption rate and temperature elevation in the human head due to overexposure to mobile phone radiation with different usage patterns*, International Journal of Heat and Mass Transfer, vol. 130, no. 3, pp. 1178–1188 (2019), DOI: [10.1016/j.ijheatmasstransfer.2018.11.031](https://doi.org/10.1016/j.ijheatmasstransfer.2018.11.031).
- [34] Pintos V.P., Ovide B.A., Munoz C., *EMC measurements in Buenos Aires metro system*, IEEE International Symposium on Electromagnetic Compatibility, Turkey, vol. 2003, no. 1, pp. 40–43 (2003), DOI: [10.1109/ICSMC2.2003.1428187](https://doi.org/10.1109/ICSMC2.2003.1428187).
- [35] Lv H.G., *Network spectrum measurement technique*, Beijing: Tsinghua University Press, pp. 23–36 (2000).
- [36] Spiegel R.J., *A review of numerical models for predicting the energy deposition and resultant thermal response of humans exposed to electromagnetic fields*, IEEE Transactions on Microwave Theory and Techniques, vol. 32, no. 8, pp. 730–746 (1984), DOI: [10.1109/TMTT.1984.1132767](https://doi.org/10.1109/TMTT.1984.1132767).
- [37] Pennes H.H., *Analysis of tissue and arterial blood temperatures in the resting human forearm*, Journal of Applied Physiology, vol. 85, no. 1, pp. 5–34 (1998), DOI: [10.1152/jap.1998.85.1.5](https://doi.org/10.1152/jap.1998.85.1.5).
- [38] Yang D., Converse M.C., Mahvi D.M., *Expanding the bioheat equation to include tissue internal water evaporation during heating*, IEEE Transactions on Biomedical Engineering, vol. 54, no. 8, pp. 1382–1388 (2007), DOI: [10.1109/TBME.2007.890740](https://doi.org/10.1109/TBME.2007.890740).